Selective discrimination and classification of G-quadruplex structures with a host–guest sensing array

DispatchDate: 23.02.2021 · ProofNo: 647, p.1

nature chemistry

ARTICLES

https://doi.org/10.1038/s41557-021-00647-9

Selective discrimination and classification of G-quadruplex structures with a host–guest sensing array

Junyi Chen[1], Briana L. Hickey[2], Linlin Wang[2], Jiwon Lee[2], Adam D. Gill[3], Alessia Favero[4,5], Roberta Pinalli[4,5], Enrico Dalcanale[4,5], Richard J. Hooley[2,3] ✉ and Wenwan Zhong[1,2]

The secondary structures of nucleic acids have an important influence on their cellular functions but can be difficult to identify and classify quickly. Here, we show that an arrayed suite of synthetic hosts and dyes is capable of fluorescence detection of oligonucleotide secondary structures. Multivariate analysis of different fluorescence enhancements—generated using cationic dyes that show affinity for both DNA G-quadruplexes and the synthetic hosts—enables discrimination between G-quadruplex structures of identical length and highly similar topological types. Different G-quadruplexes that display the same folding topology can also be easily differentiated by the number of G-quartets and sequence differences at the 3′ or 5′ ends. The array is capable of both differentiation and classification of the G-quadruplex structures at the same time. This simple non-invasive sensing method does not require the discovery and synthesis of specific G-quadruplex binding ligands, but employs a simple multicomponent approach to ensure wide applicability.

The cellular functions of nucleic acids are dependent not only on the nucleotide sequence, but also on the secondary structural architecture. Nucleotide strands can form complex 3D structures, expanding their function beyond encoding and transferring genetic information[1]. For example, uniquely folded DNA structures such as G-quadruplexes (G4s) have been found in cancer tissues and viral genomes[2] and synthetic DNA and RNA nanostructures have a wide variety of applications in synthetic biology and nanomedicine[3,4]. As such, there is a need for methods that can quickly and easily assess the structures of nucleotides of various types, not just the sequence. Although DNA folding directed by Watson–Crick base-pairing can be predicted[5], it remains challenging to analyse non-canonical structures from sequences alone. Determination of nucleic acid 3D structures can be achieved in different ways: complete structural analysis requires X-ray crystallography and/or multidimensional NMR spectroscopy[6,7], whereas simple grouping into secondary structural types is possible with circular dichroism (CD) spectroscopy[8]. These techniques have their challenges, in that they are either too time-consuming and detailed for rapid analysis (X-ray, NMR), or provide too little information (CD). A rapid, simple method that can selectively identify, differentiate and classify nucleotide secondary structures is highly desirable, but also very challenging and applying this sensor in complex biological media is even more so.

Optical sensing of RNA secondary structures can be achieved with synthetic, derivatized nucleotides[9]. This requires differential sensing, which was popularized by Anslyn for small molecule analytes[10] and has been used by others to classify the 2D and 3D structure of derivatized RNAs[11]. By incorporating dyes at multiple different positions on the RNA backbone and adding multiple small molecule effectors, array-based sensing can be exploited to classify different structural motifs and conformational changes, using multivariate analysis tools such as principal component analysis (PCA) and hierarchical cluster analysis[12]. Some beautiful examples of RNA classification have been shown, but they are not an effective method for monitoring native, unmodified oligonucleotide structures. That requires an exogenous fluorophore that must show selective responses to nucleotides and selectivity for different structural motifs, which is not simple. Some excellent work has been performed that uses fluorescence displacement assays and multivariate analysis to classify ligands that have selectivity for DNA strands with large structural differences (duplex, i-motif, G4 and so on)[13].

The greatest challenge for any sensor is to distinguish between highly similar structures in a complex mixture. DNA G4s are an excellent example of a challenging recognition target, as their overall size and the internal structure are relatively conserved. They are a common non-canonical structural motif[14,15], involving stacked guanine quartets assembled via Hoogsteen base-pair contacts and intercalated Na^+ or K^+ ions linked by loop nucleotides[16]. G4s are generally classified into three different structural types, based on the directionality of the four G strands forming the G-quadruplex (G4): parallel, antiparallel or hybrid (illustrated in Fig. 1b). As in double-stranded DNA, G4 structures have grooves, the dimensions of which are determined by the overall topology and the nature of the loops. The variations lie in the strand orientation, glycosidic angles and the directionality of the external loops[17]. These changes are not easy to detect: they are, after all, just oligomers of phosphorylated sugars oriented in different directions. CD spectroscopy can disclose the types of topology (that is parallel, antiparallel, or hybrid) but cannot recognize small structural differences in G4s of the same folding type. Although computational prediction and genomic mapping have shown a myriad of sequence motifs that could form G4 structures[18,19], conformational studies have only been conducted on a few of these sequences. This has involved the use of

[1]Environmental Toxicology Program, University of California, Riverside, CA, USA. [2]Department of Chemistry, University of California, Riverside, CA, USA. [3]Department of Biochemistry and Molecular Biology, University of California, Riverside, CA, USA. [4]Department of Chemistry, Life Sciences and Environmental Sustainability, University of Parma, Parma, Italy. [5]INSTM, UdR, Parma, Italy. ✉e-mail: richard.hooley@ucr.edu

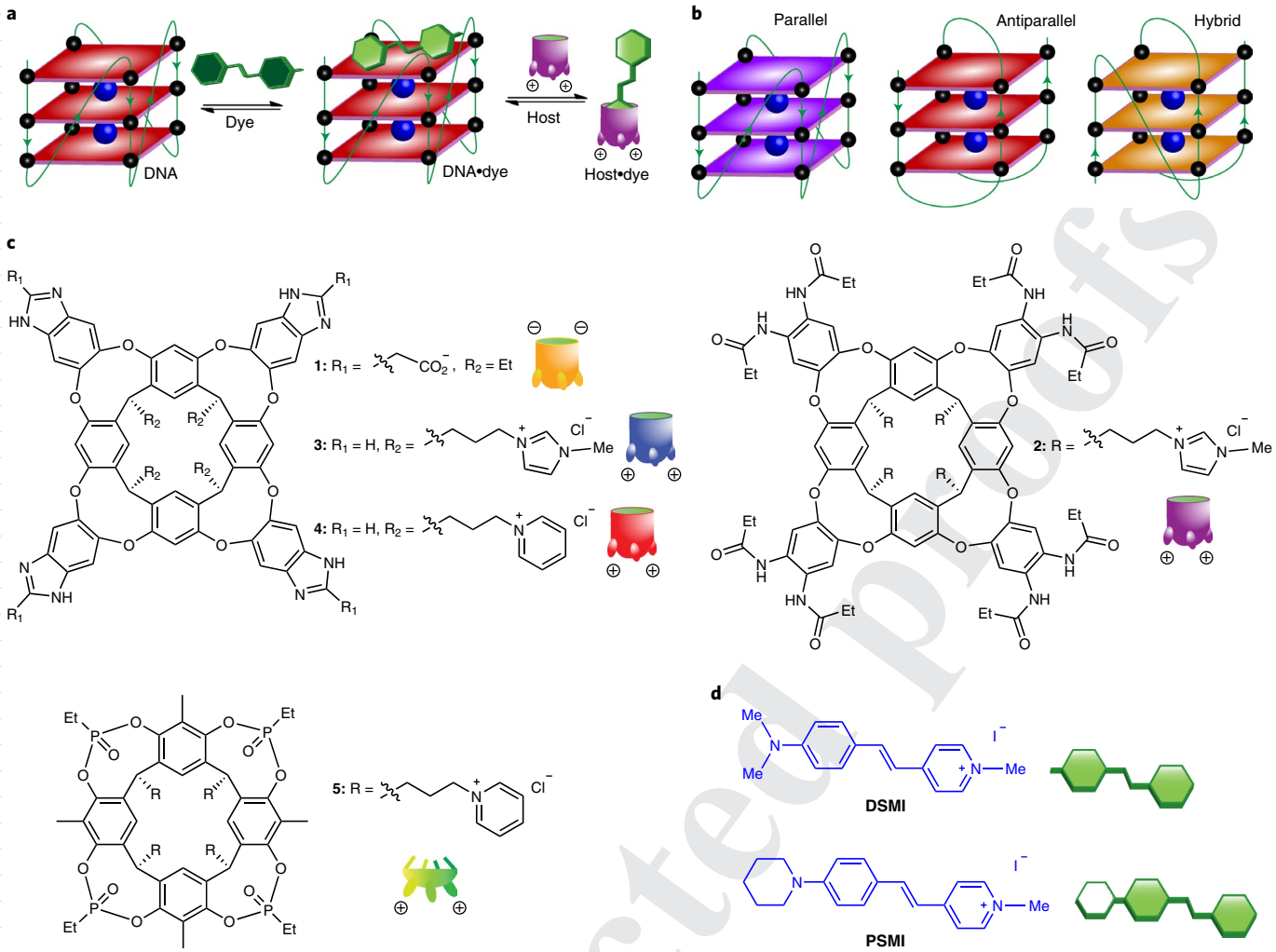

Fig. 1 | A host–guest sensor system for label-free classification and differentiation of G-quadruplex structures. a, Illustration of the supramolecular sensing concept: the cationic dyes can be bound by both the DNA targets and the various host molecules and their emission is modulated by each recognition event in a complex equilibrium. When multiple hosts and dyes are used, an array-based sensor system can be created for pattern recognition by multivariate analysis. **b**, Representation of the common DNA G-quadruplex (G4) structural motifs targeted here. **c**,**d**, Structures of hosts **1**–**5** (**c**) and dyes (**d**). Cartoon illustrations of each host/dye used in later figures are adjacent to their structures, showing the relative positions of their charged groups at the upper or lower rim. **DSMI** = *trans*-4-[4-(dimethylamino)styryl]-1-methylpyridinium iodide, **PSMI** = including *trans*-4-[4-(piperidino)styryl]-1-methylpyridinium iodide.

small molecule ligands which recognize G4s mainly through π–π stacking with the G tetrads, plus binding to the grooves or loops[20,21]. Some ligands are highly selective[21] but they are not common and not easily applied in sensing applications.

Here we show that small-molecule host–guest sensor arrays can be used to sense structural differences in unmodified DNA G-quadruplex structures, allowing both their differentiation and classification, via simple fluorescence measurements and pattern recognition. Supramolecular probes are perfectly suited to array-based pattern recognition due to their simple synthesis, ease of use and rapid access to multiple variables[22], which is essential in detecting small changes in structure. Host–guest sensor arrays have been used to monitor enzyme reactions[23,24] and analyse peptide and protein modifications[25,26]. They have rarely been applied to nucleotide sensing, because synthetic hosts often show poor affinity for oligonucleotides[27]. The solution to this challenge lies in indirect sensing: by combining an arrayed suite of host molecules with multiple dye candidates that can bind both the hosts and the target oligonucleotides, small changes in target structure can be selectively detected.

Results and discussion

Design of host–guest sensor system and analysis of the sensing mechanism. Pattern recognition-based sensing requires multiple different components that show variable fluorescence responses to the target, in this case oligonucleotide strands. The basic design principle is shown in Fig. 1a and exploits hosts and dye guests that have variable affinity for each other and with the target oligonucleotides. The sensor components consist of cationic dye molecules that can bind to DNA structures (Fig. 1d), as well as a series of synthetic host molecules that can also competitively bind these dyes while modulating their fluorescence (Fig. 1c). Extended Data Fig. 1 shows minimized structures of the host–guest complexes. The styrylpyridinium **DSMI** and **PSMI** fluorophores[28,29] are cationic, yet water soluble and similar in structure to known oligonucleotide ligands[30]. They vary only in the size of headgroup and have similar fluorescence properties. The slightly varying size and shape should confer small differences in nucleotide affinity, while maintaining similar detection ranges.

The second component is a set of water soluble host molecules (cavitands) that can bind to the fluorophores and modulate their

emission. Cavitand hosts **1–5** (Fig. 1c) were used, all of which should show affinity for the dyes, allowing a competition between the G4 and the host. These sensor components can then be combined in an array for pattern recognition analysis. Tetraanionic host **1** (ref. [31]) is known to bind **DSMI** (ref. [28]) and **PSMI** (ref. [29]) and has been extensively used in biosensing applications[32,33]. Cationic cavitand **2** (ref. [29]) has a similar cavity size to **1**, but displays imidazolium groups at the lower rim for water solubility. Similarly, the benzimidazole cavitands **3** and **4** (ref. [34]) are derivatives of **1** with cationic groups at the lower rim. Finally, the shallow phosphonate cavitand **5** (ref. [35]) was used, as this also binds organic cations[36].

The initial test was to determine whether the dyes could show variable response to G-quadruplexes in the presence of the different hosts. The two dyes were added to a suite of DNA structures, followed by increasing concentrations of hosts **1–5** and the fluorescence response curves recorded. Eight different DNA structures were initially tested: four single-stranded DNAs (A20, G20, T20 and C20) and four G4 structures. c-kit1 and c-myc 2345 are parallel G4s, bcl-2 2345 forms a hybrid structure and TBA is antiparallel[37]. Gel electrophoresis confirmed that the G4 strands all formed unimolecular folded structures and their folding topologies were all validated by CD (see Supplementary Figs. 1–6).

Both **PSMI** and **DSMI** showed fluorescence enhancements up to threefold to sixfold upon addition to all the DNAs. The changes in the dyes by themselves with different G4 structures were not substantially different, so simple addition of the individual dyes to the DNAs does not provide selectivity. However, upon addition of the cavitands to the dye–DNA mixtures, significant variations in emission properties can be immediately observed (see Fig. 2a–c). The responses are quite complex and vary with host in three broad types: the responses for anionic host **1**, shallow host **5** and cationic hosts **2–4**. To account for the effects of the DNA on the emission profiles, two types of fluorescence plot are shown: the raw fluorescence counts (Extended Data Fig. 2a,c,e) and plots normalized to the response of cavitand–dye in the absence of DNA (Fig. 2a–c and Extended Data Fig. 2b,d,f). This normalization removes the effect of the host–dye emission on the signal and focuses solely on the effects of changing DNA target. For full fluorescence plots for all host–dye combinations, see Supplementary Figs. 18 and 19.

The normalized response for host **1** is quite simple (Fig. 2a), as the emission is lowered with increasing host concentration. However, the profiles for the cationic hosts are different (Fig. 2b,c, Extended Data Fig. 2c–f and Supplementary Figs. 18 and 19). When hosts **2–5** are added to the DNA•dye complexes, an initial increase in emission is observed at very low concentration, followed by a fluorescence decrease. After 1 μM host is added, no effects on the normalized emission are seen with hosts **2–4**. By contrast, phosphonate host **5** causes a slight quenching of the dye upon host•dye complex formation (Extended Data Fig. 2e)[38]. The fluorescence responses for the two dyes are slightly different, which provides a simple array variable: small changes in dye can cause small, reproducible changes in emission.

To rationalize these effects, we determined the binding affinities[39] between PSMI/DSMI, the hosts and the c-myc 2345 G4 (see Table 1 and Supplementary Figs. 14–16). Both dyes bind strongly yet variably to each host with dissociation constants K_d from 2.8 μM (DSMI•5) to 72.3 μM (DSMI•2). The dyes also bind to the DNA G4, with K_d of the order of 100–250 μM for both **DSMI** and **PSMI**. In each case, the G4–dye affinity was lower than the host–dye affinity, corroborating the theory that the hosts extract the dyes from the DNA.

These results suggest multiple sensing mechanisms, as shown in abbreviated form in Fig. 2d. Cavitand **1** competitively binds the fluorophore, removing it from the DNA and causing an initial decrease in normalized fluorescence. Cationic hosts **2–5** are slightly different: the hosts competitively bind the dyes and at high concentrations this eliminates any dye•DNA binding. At low concentrations, the arced fluorescence plots indicate that a second mechanism is present, presumably due to the cationic hosts also interacting with the DNA. Three states can be in equilibrium: DNA•dye, host•dye and DNA•dye•host, whereby the host causes an additional enhancement in fluorescence of the dye. This is consistent for all cationic hosts **2–5** and only occurs at low [host]. It is not completely clear why the 'arcing' in the fluorescence titrations occurs for the cationic hosts. Some plausible options are that either the dye•host complex associates with the DNA ('state 2', Fig. 2d), causing an increase in emission, or the added host interacts with the dye•DNA complex ('state 1'), or both.

Discriminating different DNA structures with the sensor array. While there are multiple mechanistic possibilities for the emission differences with variable hosts and guests, the important conclusion for differential sensing purposes is that the responses are small but highly sensitive to DNA structure. As such, we constructed four different host•dye arrays of varying sizes. The host•dye concentrations were chosen to give the optimal response differences. The Type 1 array (6 component) uses **DSMI** dye and hosts **1–5**, along with no host and the Type 2 array (6 component) uses **PSMI** dye with hosts **1–5**, along with no host. Two larger arrays were also used: the 10-component array uses **DSMI** and **PSMI** dyes with hosts **1–5** and the 12-component array consists of both Type 1 and Type 2 arrays. For full details, see Methods.

Exposing the eight different DNA targets to the full 12-component array gives the response plot in Fig. 3a, which illustrates the highly variable responses possible. These responses were subjected to PCA and the scores plot is shown in Fig. 3b. This shows that the array can fully discriminate all 8 strands tested, with all the repeated measurements included within the 95% confidence ellipses and no overlap detected between these ellipses. Importantly, as well as distinguishing large differences between structured/unstructured DNA strands, the sensor array could discriminate two parallel G4 strands of identical length, c-kit1 and c-myc 2345, indicating the array is sensitive to small changes in sequence and structure. Another notable phenomenon is that the G20 strand is well separated from the unstructured A/T/C20 strands, which is presumably due to the formation of higher-order structures in situ[40]. The limit of detection was excellent and the array can work within a wide DNA concentration range of 3–500 nM (see Supplementary Tables 2 and 3 and Supplementary Figs. 20 and 21).

In addition to discriminating between DNAs with large structural differences, much more subtle selectivity is possible. The hybrid (bcl-2 2345) and parallel (c-myc 2345, c-kit1) G4 structures were well separated from each other, but resided in the same general area of the scores plot. This clustering matches their similar sizes: these three G4s are all 22 or 23 nucleotides (nt) long and contain 3 stacks of G-quartets. The most notable difference was the 2-stack antiparallel strand TBA, which is far shorter than the other G4s (15 nt) and was located far apart from the other 3-stack antiparallel G4s in the scores plot. This shows that the array can discriminate between G4s with different sizes as well as G4s with different topology types, despite their similar structures.

The combination of dyes and hosts in the array is essential: if the two dyes are used in the absence of host, minimal nucleotide discrimination is seen (see Supplementary Fig. 25). To determine which hosts had the greatest effect on G4 differentiation, we systematically removed array components and examined the grouping effect (see Supplementary Figs. 22–27). For the simple sensing shown in Fig. 3, good discrimination can be achieved with 6-component arrays, using a single dye (either **PSMI** or **DSMI**, although **PSMI** is more effective) with the 5 hosts. Reducing the number of hosts decreased the discrimination power, although the combination of DSMI/PSMI and cavitand **2** was surprisingly effective (see Supplementary Fig. 26).

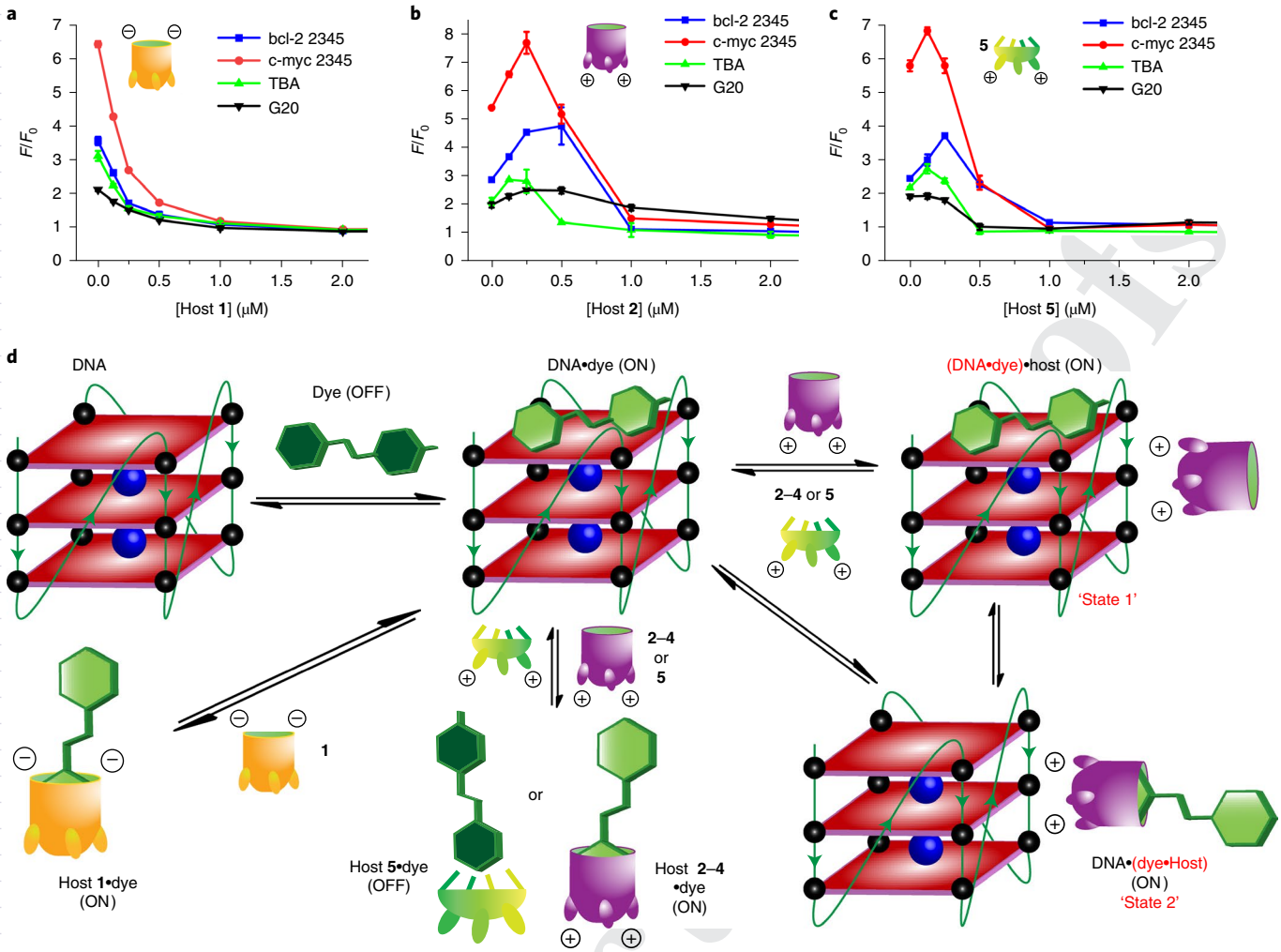

Fig. 2 | Effect of DNA strands on the emission profiles of various host–dye complexes. a–c, Normalized fluorescence response curves corresponding to the emission of **DSMI** dye in the presence of different DNA strands upon titration of hosts **1** (**a**), **2** (**b**) and **5** (**c**), illustrating the effect of the DNA structure on the emission of the various host–guest complexes. [**DSMI**] = 0.625 μM, [DNA] = 0.1 μM, [host] = 0-2 μM, 10 mM KH_2PO_4/K_2HPO_4 buffer, 1 mM EDTA, pH 7.4, Ex/Em = 485 nm/605 nm. The normalization process defines F_0 as the emission at [DNA] = 0. The raw, unnormalized plots corresponding to this data can be found in Extended Data Fig. 2, along with expanded versions of the normalized plots. For the full suite of titration plots with all hosts **1–5** and both dyes, see Supplementary Figs. 18 and 19. Error bars represent the standard deviation of three repeated measurements. **d**, Illustration of the various equilibria present when the hosts and dyes are exposed to DNA G-quadruplexes. These multiple recognition events allow application of this system in an array-based format for differentiation of different G4s (see Figs. 3–5).

Discrimination and classification of structurally similar DNA targets. This simple screen illustrates the abilities of the host–guest array: the different molecular recognition events, combined with varying fluorescence responses, allow differentiation of nucleotide structures, even those with similar structural characteristics. The next, far more stringent test was to see if the sensor could discriminate between a series of different yet structurally similar G4 structures and whether it could also provide classification. A suite of 23 different G4s in 3 family types with strand lengths from 15 to 26 nt was tested (for full sequences see Supplementary Table 1). This included six parallel (c-kit1, c-kit2, pu22, c-myc 2345, EAD4 and PS5.M), eight antiparallel (TBA, Bom19, 2KF8, 442A3, TTT-L13, 2KKA, TA2 and 6FTU) and nine hybrid structures (AG22, bcl-2 2345, TP3, wtTel23, wtTel24, wtTel26, Tel 26, Telo24 and H24). The topologies of these strands were confirmed by CD analysis and each strand was confirmed to be a unimolecular G4 by gel electrophoresis (Supplementary Figs. 5 and 6).

As most of these G4 targets are highly similar in size and global structure, we employed the full 12-component array to deliver the most powerful discrimination possible (see Supplementary Fig. 28 for full fluorescence response plots). The fluorescence data were collected as above and the responses were analysed by a series of multivariate analysis tools (Fig. 4). For clarity, Fig. 4a shows the average fluorescence change from five repeated measurements on each G4 as a single plot point. The full suite of data points is shown in Extended Data Fig. 3, including error ellipses, but the simplified plot in Fig. 4a illustrates the results nicely. The clear outcome of the PCA plots is that the sensor can easily discriminate between the parallel G4 structures (six different G4s, illustrated in red) from all the other entries. The discrimination is remarkable, as three of the G4s (c-kit1, pu22, c-myc 2345) have exactly the same strand length (22 nt) and the same topology, yet are fully separated on the scores plot. The discrimination between the hybrid and antiparallel G4 structures is at first glance less impressive, but closer inspection leads to some interesting observations. The grouping of the hybrid structures is quite clear and is shown in blue in Fig. 4a, grouped around the centrepoint of the plot. However, there is significant variation in the positions of the antiparallel strands, with four G4s (TTT-L3,

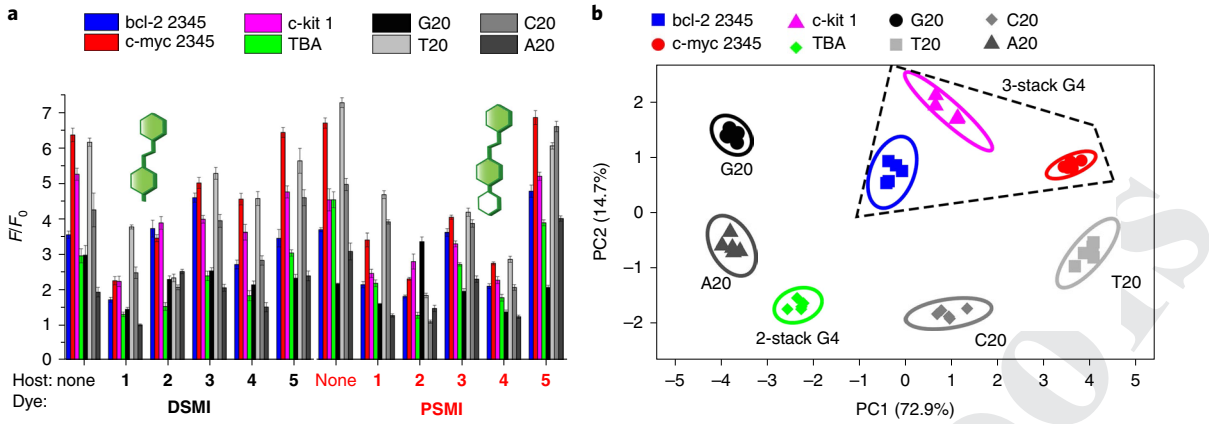

Fig. 3 | Selective array-based sensing of variable DNA structures. a, Fluorescence (*F*) responses upon addition of the eight DNA strands to the host•dye sensor components, F_0 = emission at [DNA] = 0. Each array component shows a different fluorescence response and this array of responses can be subjected to multivariate analysis to differentiate the DNA structures. **b**, PCA scores plot generated from the data in **a**, using the 12-component array (the combination of Type 1 and Type 2 arrays). The scores plot of the first two principal components, in total summarizing more than 87% of the variation contained in the data, provides a visualization of how the 8 DNA strands can be differentiated by our array. Different strands are well separated from each other, with the five repeats of the same strand clustered tightly together. Error bars indicate standard deviation of five repeated measurements. [Dye] = 0.625 μM in both arrays, with the Type 1 array using **DSMI** and [**1**, **4**, or **5**] = 0.25 μM or [**2** or **3**] = 0.50 μM, or no cavitand and the Type 2 array using **PSMI** and [**1**, **3**, or **5**] = 0.25 μM, [**2**] = 1.0 μM, or [**4**] = 0.50 μM, or no cavitand. [DNA] = 0.1 μM, 10 mM KH_2PO_4/K_2HPO_4 buffer, 1 mM EDTA, pH 7.4, Ex/Em = 485 nm/605 nm. Ellipses indicate 95% confidence.

2KKA, 442 A3 and 2KF8) co-located with the hybrid structures and the other four structures in two separate groups (6FTU/TA2 and TBA/Bom19). The challenges in differentiating the hybrid and antiparallel structures can be easily explained by their structural similarities. Hybrid and antiparallel G4s both contain one or two of the four G strands in an orientation opposite the others and both display *anti* and *syn* guanines. They are even, in certain literature cases, considered as a single topology group[16,18]. The discrimination shown between certain hybrid and antiparallel strands in our screen is dependent on their length. The antiparallel and hybrid G4s that are co-located close to each other are all of similar lengths (22–26 nt) and all display three G-quartet stacks. The outlier antiparallel structures vary in the number of G-quartet stacks, either 2 (TBA and Bom19) or 4 (6FTU and TA2) and these larger variations in structure are fully separated from the 3-stack G-quartets (either antiparallel or hybrid). In addition, some impressive discrimination effects can be seen for these G4s. Although 2KKA has high sequence similarity with 2KF8, AG22, wtTel23 and wtTel24 (varying only by the absence of one T or one A on the 3′ or 5′ end), it is well separated from the other strands in the PC2 axis. Similar differentiation is also observed between Tel26 and wtTel26, as well as between Telo24 and H24. When an additional component was added to the PCA (that is PC3, accounting for 4.46% of the overall variation in the dataset) even greater separation between the 3-stack hybrid and antiparallel structures was seen: 442 A3 was well separated from bcl-2 2345 (Fig. 4b). The array can differentiate these G4 structures based on multiple secondary structural features, including topology, number of G-quartet stacks and the underlying base sequence. Dissecting the contribution of individual array elements shows that changing the host is most important for differentiating the structures by their topology, while the different dyes contribute more towards revealing differences in stack numbers and sequences (see Supplementary Figs. 29 and 30 for PCA plots with varying array elements). This illustrates the power of the array concept: by introducing (or removing) individual array components, the sensor can be tailored for specific targets and is not restricted to one type of DNA structure.

The strong differentiation between different G4 topologies shown by the array suggests that it could also classify the G4s by their topology. To validate this, the responses were also subjected to canonical discriminant analysis (CDA) (Fig. 4c)[12]. Whereas PCA is an unsupervised classification tool that finds the greatest variance between samples and clusters the samples with a smaller variance, CDA is supervised in classification: the class of each sample (that is the topology of each G4) is included to maximize class discrimination. As such, the unsupervised PCA confirms differentiation of different G4 sequences, but the supervised CDA analyses whether the array can classify the G4s by topology. In this case, the raw data with the full 12-element array (including all 5 repeats) for all 23 G4 structures were used as the input (a total of 115 samples classified by 12 characteristics), together with their topology information. The results are extremely impressive: the canonical scores plot (Fig. 4c) clearly shows that the targets are robustly classified into the three expected topology groups, parallel, hybrid and antiparallel (shown in red, blue and green respectively in Fig. 4c), with 114 out of 115 samples assigned to the correct topology. Only 1 sample in the hybrid group was wrongly assigned to antiparallel (Fig. 4d), an error rate in classification of 0.7%. In addition, *k*-fold ($k = 8$) cross-validation analysis, in which 1/8 of the observations were removed from the data set and treated as unknowns, led to an average precision rate of 98.21%. This analysis corroborates the PCA results well and validates the power of the sensor array in classifying highly similar G4 sequences by topology type.

Table 1 | Binding affinities between dyes and hosts/DNA[a]

Dye	K_d (1) (μM)[b]	K_d (2) (μM)[b]	K_d (3) (μM)[b]	K_d (4) (μM)[b]	K_d (5) (μM)[b]	K_d (c-myc 2345) (μM)[c]
DSMI	5.3 ± 0.4	72.3 ± 2.4	6.1 ± 1.3	20.3 ± 1.5	2.8 ± 1.4	247 ± 68
PSMI	8.2 ± 0.9	51.7 ± 2.8	8.6 ± 1.3	5.8 ± 1.22	3.3 ± 1.8	112 ± 27

[a]10 mM KH_2PO_4/K_2HPO_4 buffer, 1 mM EDTA, pH 7.4. [b]Measured by fluorescence titrations[39], with [dye] = 0.625 μM for hosts **1**–**4** and 10 μM for host **5**. [c]Measured by isothermal titration calorimetry at 25 °C, with increasing amounts of **DSMI** added to 10 μM c-myc 2345 or **PSMI** to 40 μM c-myc 2345.

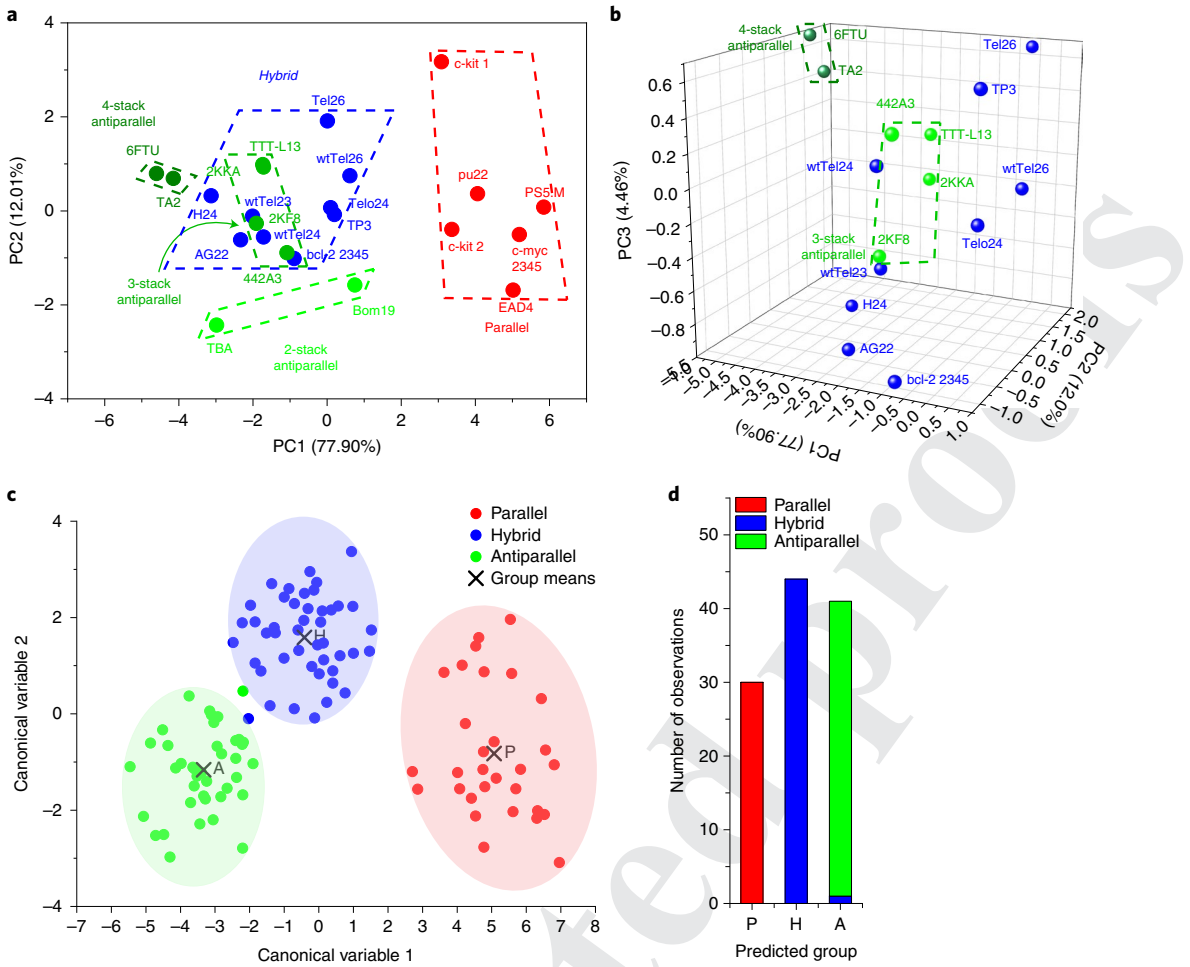

Fig. 4 | Classification and discrimination of a suite of 23 G-quadruplex structures. a, 2D PCA scores plot of the first two principal components (PCs) generated from the fluorescence responses of 23 G4 strands to the sensing array. Each point is the average of five repeated measurements (see Extended Data Fig. 3 for the individual repeats). PC1 and PC2 in total summarize close to 90% of the variation contained in the data. Their scores plot illustrates that all the parallel G4s (red dots) are located close to each other, but are distant from the hybrid and antiparallel ones. The 3-stack antiparallel strands cannot be separated from some of the 3-stack hybrid G4s, but the 4- and 2-stack antiparallel G4s can be differentiated from the 3-stack strands on this plot. **b**, 3D PCA scores plot generated from the same data as in **a**, illustrating only the hybrid (blue) and antiparallel (green) G4 strands. The third PC axis better illustrates the differentiation of the 2-stack and 3-stack antiparallel G4s. **c**, Canonical scores plot resulting from CDA of the individual responses from the 12 array elements to the 115 samples grouped by topology. The scores plot illustrates clear grouping of most of the 115 samples into the correct topology class, except for one hybrid G4. **d**, Tabulation of the CDA results to illustrate the classification error rate of 1/115 samples. Sensor conditions identical to those described in Fig. 3; 12-component array used. Parallel G4s labelled in red, hybrid G4s labelled in blue, antiparallel G4s labelled in green.

Broadening the sensing scope. The discrimination tests were then performed in more complex media (Supplementary Figs. 32–39). The sensor was completely tolerant to the presence of small saccharides, with no loss of performance in the presence of 20 μM lactose. Most impressively, the sensor remained effective in the presence of 5% fetal bovine serum and full discrimination between the initial 8 targets (A/G/T/C20, c-kit1, c-myc 2345, bcl-2 2345 and TBA) was possible with the Type 1 array (Supplementary Fig. 33). Greater serum concentrations reduced the effectiveness of the sensing, but this is to be expected considering the variety of interfering molecules in fetal bovine serum. Cationic proteins such as lysozyme were the greatest interferents (Supplementary Figs. 34–37) and the array could only tolerate 0.1 μM lysozyme before losing selectivity.

As G-quadruplexes use alkali metal cations as structural components, changing the nature of the cation (from K^+ to Na^+) can sometimes cause a change in G4 topology. Notably, AG22 displays a hybrid quadruplex structure in potassium phosphate buffer, but switches to an antiparallel structure in sodium phosphate[16,41]. To determine whether the sensor array could detect these changes, we repeated the fluorescence measurements for a series of G4s in either Na^+ or K^+ phosphate buffer, using the compressed Type 1 array with **DSMI** as dye. In this case, five G4 structures were chosen: AG22, with TBA, c-myc 2345, c-kit1 and bcl-2 2345 as controls. The sensor results are shown in Fig. 5a: in the PCA scores plot in K^+ buffer, the data points corresponding to AG22 are in close proximity to those of the hybrid G4 control of bcl-2 2345, with the 95% confidence ellipses overlapping significantly. The parallel and antiparallel controls are fully distinguished. When the same measurements are made in buffer containing Na^+ ions, the changes become obvious: no longer is AG22 co-located with the hybrid bcl-2 2345, but it moves into close proximity with the antiparallel TBA. These observations were corroborated by the CD spectra (Supplementary Fig. 4). While the sensor is sensitive to changes in buffer, it is still fully capable of sensing the hybrid→antiparallel structural change of AG22, which was one of the most challenging conformational

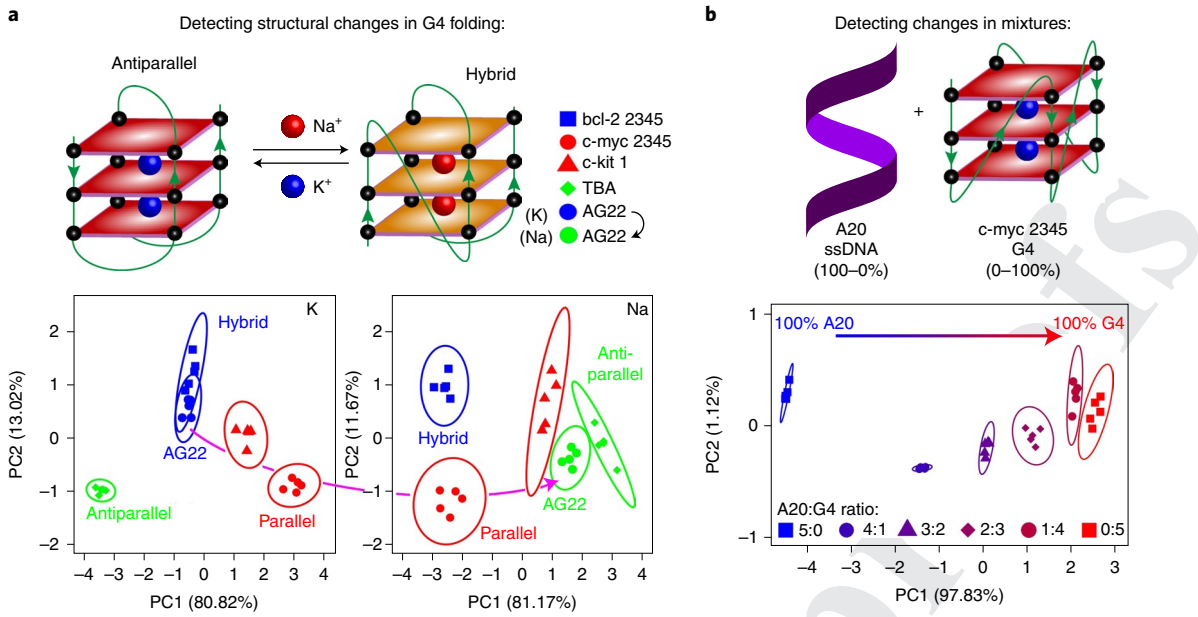

Fig. 5 | More complex sensing with the array, which can detect structural topology switching and changing concentration of specific G4s in a mixture. **a**, Sensing the structural change of the AG22 G4 from hybrid to antiparallel with different structural cations (K^+ (left) to Na^+ (right)). PCA scores plot from the fluorescence responses of five G4 strands, AG22 and four controls ([DNA] = 0.1 μM) in either 10 mM KH_2PO_4/K_2HPO_4 or NaH_2PO_4/Na_2HPO_4 buffer, Ex/Em = 485 nm/605 nm. In the PCA scores plot generated from DNAs in a K^+ buffer, AG22 is co-located with the hybrid G4 of bcl-2 2345, but the plot from DNAs in the Na^+ buffer shows AG22 next to the antiparallel G4 of TBA, confirming the topology switch. Both scores plots show good discrimination of the G4s with different topology, with the two first principal components summarizing more than 93% of the total variance of the data. **b**, Detection of varying concentration of a specific G4 in a mixture of different DNAs. PCA scores plot from the fluorescence responses of solutions containing various molar ratios of the c-myc 2345 G4:polyA20 strand ([total DNA] = 0.5 μM) in 10 mM KH_2PO_4/K_2HPO_4 buffer, Ex/Em = 485 nm/600 nm. Both plots were generated using the Type 1 sensing array; all buffers with 1 mM EDTA, at pH = 7.4. The first two principal components that summarize close to 99% of the overall data variance. The scores plot shows the mixtures containing higher proportions of G4 moving to the right of the plot with higher PC1 values, while the ones having lower G4 contents moving to the left, with lower PC1 values. Fluorescence data for these plots can be found in Supplementary Fig. 40.

variations to detect among our 23 G4 candidates in identical buffer conditions.

The sensor can also detect changes in G4 concentration in a mixture of oligonucleotides. The c-myc 2345 G4 was combined with the A20 single-stranded DNA strand in varying proportions and added to a solution of the compressed Type 1 array with **DSMI** as the dye. The fluorescence responses (Supplementary Fig. 40) were subjected to PCA and the scores plot is shown in Fig. 5b. As the proportion of A20/c-myc 2345 varies, the signals on the scores plot move towards the relevant signals for 100% A20/c-myc 2345 (shown in blue and red respectively), with the changes dominated by the position on PC1. Even in the presence of competing nucleotides, the selectivity of the sensor for the folded structure is retained.

Conclusions

Here we have shown that an arrayed suite of synthetic hosts and dyes is capable of sensing oligonucleotide secondary structures. Multiple recognition mechanisms can be exploited to create a unique sensing fingerprint consisting of variable fluorescence enhancements in the presence of different DNA strands. Multivariate analysis of these sensing fingerprints enables discrimination between DNA structures, which can be as different as single stranded A20 and G20, or as similar as G-quadruplex strands that vary only slightly in structure and size.

Most importantly, the array is able to both differentiate and classify the G4 structures at the same time. Simply differentiating between different G4 types has limited utility by itself: the ability to differentiate between different G4 structures while also enabling their classification is essential for detecting the presence of specific secondary structural motifs as disease markers, for example. Whereas CD spectroscopy can quickly identify folding topology, it is incapable of distinguishing between different G4 structures of the same folding type. Mass spectrometry and sequencing techniques can easily detect differences in size, but are poor at determining the secondary structure in solution. Our array is capable of both types of analysis at the same time in a simple non-invasive manner, which requires little sample and does not require discovery and synthesis of specific ligand targets for each oligonucleotide type. The selectivity is excellent: different G4s that display the same folding topology can be easily differentiated by the number of G-quartets and sequence differences. Our array can even detect changes in G4 folding pattern in different types of complex medium, in the presence of interfering small molecules and in mixtures of nucleotides. This method could potentially be employed in computational modelling to show close correlation between sequence and structure. This could pave the way to accurate prediction of nucleic acid folding based on its sequence and their fluorescence responses in our array.

Online content

Any methods, additional references, Nature Research reporting summaries, source data, extended data, supplementary information, acknowledgements, peer review information; details of author contributions and competing interests; and statements of data and code availability are available at https://doi.org/10.1038/s41557-021-00647-9.

Received: 14 January 2020; Accepted: 27 January 2021;

References

1. Belmont, P., Constant, J.-F. & Demeunynck, M. Nucleic acid conformation diversity: from structure to function and regulation. *Chem. Soc. Rev.* **30**, 70–81 (2001).
2. Balasubramanian, S., Hurley, L. H. & Neidle, S. Targeting G-quadruplexes in gene promoters: a novel anticancer strategy? *Nat. Rev. Drug Discovery* **10**, 261–275 (2011).
3. Seeman, N. C. & Sleiman, H. F. DNA nanotechnology. *Nat. Rev. Mater.* **3**, 17068 (2017).
4. Pinheiro, A. V., Han, D., Shih, W. M. & Yan, H. Challenges and opportunities for structural DNA nanotechnology. *Nat. Nanotechnol.* **6**, 763–772 (2011).
5. Jaeger, L. & Chworos, A. The architectonics of programmable RNA and DNA nanostructures. *Curr. Opin. Struct. Biol.* **16**, 531–543 (2006).
6. Winnerdy, F. R. et al. NMR solution and X-ray crystal structures of a DNA containing both right-and left-handed parallel-stranded G-quadruplexes. *Nucleic Acids Res.* **47**, 8272–8281 (2019).
7. Salgado, G. F., Cazenave, C., Kerkour, A. & Mergny, J.-L. G-quadruplex DNA and ligand interaction in living cells using NMR spectroscopy. *Chem. Sci.* **6**, 3314–3320 (2015).
8. del Villar-Guerra, R., Trent, J. O. & Chaires, J. B. G-quadruplex secondary structure obtained from circular dichroism spectroscopy. *Angew. Chem. Int. Ed.* **57**, 7171–7175 (2018).
9. Eubanks, C. S., Forte, J. E., Kapral, G. J. & Hargrove, A. E. Small molecule-based pattern recognition to classify RNA structure. *J. Am. Chem. Soc.* **139**, 409–416 (2017).
10. You, L., Zha, D. & Anslyn, E. V. Recent advances in supramolecular analytical chemistry using optical sensing. *Chem. Rev.* **115**, 7840–7892 (2015).
11. Eubanks, C. S. et al. Visualizing RNA conformational changes via pattern recognition of RNA by small molecules. *J. Am. Chem. Soc.* **141**, 5692–5698 (2019).
12. Stewart, S., Ivy, M. A. & Anslyn, E. V. The use of principal component analysis and discriminant analysis in differential sensing routines. *Chem. Soc. Rev.* **43**, 70–84 (2014).
13. del Villar-Guerra, R., Gray, R. D., Trent, J. O. & Chaires, J. B. A rapid fluorescent indicator displacement assay and principal component/cluster data analysis for determination of ligand–nucleic acid structural selectivity. *Nucleic Acids Res.* **46**, e41 (2018).
14. Huppert, J. L. Four-stranded nucleic acids: structure, function and targeting of G-quadruplexes. *Chem. Soc. Rev.* **37**, 1375–1384 (2008).
15. Bochman, M. L., Paeschke, K. & Zakian, V. A. DNA secondary structures: stability and function of G-quadruplex structures. *Nat. Rev. Genet.* **13**, 770–780 (2012).
16. Burge, S. et al. sequence, topology and structure. *Nucleic Acids Res.* **34**, 5402–5415 (2006).
17. Dolinnaya, N. G., Ogloblina, A. M. & Yakubovskaya, M. G. Structure, properties, and biological relevance of the DNA and RNA G-quadruplexes: Overview 50 years after their discovery. *Biochemistry* **81**, 1602–1649 (2016).
18. Kwok, C. K. & Merrick, C. J. G-quadruplexes: prediction, characterization, and biological application. *Trends Biotechnol.* **35**, 997–1013 (2017).
19. Puig Lombardi, E. & Londoño-Vallejo, A. A guide to computational methods for G-quadruplex prediction. *Nucleic Acids Res.* **48**, 1–15 (2020).
20. Zuffo, M. et al. More is not always better: finding the right trade-off between affinity and selectivity of a G-quadruplex ligand. *Nucleic Acids Res.* **46**, e115 (2018).
21. Felsenstein, K. M. et al. Small molecule microarrays enable the identification of a selective, quadruplex-binding inhibitor of MYC expression. *ACS Chem. Biol.* **11**, 139–148 (2016).
22. Pinalli, R., Pedrini, A. & Dalcanale, E. Biochemical sensing with macrocyclic receptors. *Chem. Soc. Rev.* **47**, 7006–7026 (2018).
23. Dsouza, R. N., Hennig, A. & Nau, W. M. Supramolecular tandem enzyme assays. *Chem. Eur. J.* **18**, 3444–3459 (2012).
24. Hennig, A., Bakirci, H. & Nau, W. M. Label-free continuous enzyme assays with macrocycle-fluorescent dye complexes. *Nat. Methods* **4**, 629–632 (2007).
25. Peacor, B. C., Ramsay, C. M. & Waters, M. L. Fluorogenic sensor platform for the histone code using receptors from dynamic combinatorial libraries. *Chem. Sci.* **8**, 1422–1428 (2017).
26. Minaker, S. A., Daze, K. D., Ma, M. C. F. & Hof, F. Antibody-free reading of the histone code using a simple chemical sensor array. *J. Am. Chem. Soc.* **134**, 11674–11680 (2012).
27. Florea, M. & Nau, W. M. Implementation of anion-receptor macrocycles in supramolecular tandem assays for enzymes involving nucleotides as substrates, products, and cofactors. *Org. Biomol. Chem.* **8**, 1033–1039 (2010).
28. Liu, Y. et al. Selective heavy element sensing with a simple host–guest fluorescent array. *Anal. Chem.* **89**, 11113–11121 (2017).
29. Gill, A. D. et al. Sensing of citrulline modifications in histone peptides by deep cavitand hosts. *Chem. Commun.* **55**, 13259–13262 (2019).
30. Murat, P., Singh, Y. & Defrancq, E. Methods for investigating G-quadruplex DNA/ligand interactions. *Chem. Soc. Rev.* **40**, 5293–5307 (2011).
31. Biros, S. M., Ullrich, E. C., Hof, F., Trembleau, L. & Rebek, J. Kinetically stable complexes in water: the role of hydration and hydrophobicity. *J. Am. Chem. Soc.* **126**, 2870–2876 (2004).
32. Liu, Y. et al. Site-selective sensing of histone methylation enzyme activity via an arrayed supramolecular tandem assay. *J. Am. Chem. Soc.* **139**, 10964–10967 (2017).
33. Liu, Y. et al. Selective sensing of phosphorylated peptides and monitoring kinase and phosphatase activity with a supramolecular tandem assay. *J. Am. Chem. Soc.* **140**, 13869–13877 (2018).
34. Mosca, S., Yu, Y. & Rebek, J. Preparative scale and convenient synthesis of a water-soluble, deep cavitand. *Nat. Protoc.* **11**, 1371–1387 (2016).
35. Pinalli, R. et al. The origin of selectivity in the complexation of *N*-methyl amino acids by tetraphosphonate cavitands. *J. Am. Chem. Soc.* **138**, 8569–8580 (2016).
36. Menozzi, D. et al. Thermodynamics of host–guest interactions between methylpyridinium salts and phosphonate cavitands. *Supramol. Chem.* **22**, 768–775 (2010).
37. Yang, Q. et al. Verification of specific G-quadruplex structure by using a novel cyanine dye supramolecular assembly: II. The binding characterization with specific intramolecular G-quadruplex and the recognizing mechanism. *Nucleic Acids Res.* **38**, 1022–1033 (2010).
38. Früh, A. E., Artoni, F., Brighenti, R. & Dalcanale, E. Strain field self-diagnostic Poly(dimethylsiloxane) elastomers. *Chem. Mater.* **29**, 7450–7467 (2017).
39. Thordarson, P. Determining association constants from titration experiments in supramolecular chemistry. *Chem. Soc. Rev.* **40**, 1305–1323 (2011).
40. Sengar, A., Heddi, B. & Phan, A. T. Formation of G-quadruplexes in poly-G sequences: structure of a propeller-type parallel-stranded G-quadruplex formed by a G15 stretch. *Biochemistry* **53**, 7718–7723 (2014).
41. Ambrus, A. et al. Human telomeric sequence forms a hybrid-type intramolecular G-quadruplex structure with mixed parallel/antiparallel strands in potassium solution. *Nucleic Acids Res.* **34**, 2723–2735 (2006).

Methods

General details. Cavitands 1 (ref. [31]), 2 (ref. [29]), 3 (ref. [34]) and 4 (ref. [34]), as well as phosphonate cavitand **5** (ref. [35]) and **PSMI** fluorophore[29] were synthesized according to literature procedures. NMR spectra were recorded on a Bruker Avance NEO 400 MHz. Deuterated NMR solvents were obtained from Cambridge Isotope Laboratories, Inc. and were used without further purification. All other materials, including *trans*-4-[4-(dimethylamino)styryl]-1-methylpyridinium iodide (**DSMI**) were obtained from Aldrich or Fisher Scientific and were used as received. Solvents were dried through a commercial solvent purification system (Pure Process Technologies, Inc.). Oligonucleotides were purchased from Integrated DNA Technologies with standard desalting and no further purification. The sequence and topology information of the oligonucleotides is given in Supplementary Table 1. All DNA solutions were prepared in 10 mM K_2HPO_4/KH_2PO_4 or Na_2HPO_4/NaH_2PO_4 buffer at pH 7.4, both containing 1 mM EDTA (referred to as the K^+ or Na^+ buffer in the text) and their concentrations were determined with a NanoDrop 2000 (Thermo Fisher Scientific) using the corresponding molar extinction coefficients provided by Integrated DNA Technologies after background subtraction. Before fluorescence or CD measurement, the DNAs were diluted to 1 μM with the K^+ or Na^+ buffer and re-annealed to form the most stable folding topology, in which the DNA solution was heated at 95 °C for 5 min and then kept at 4 °C overnight. Fluorescence measurements were performed with a Perkin Elmer Wallac 1420 Victor 2 Microplate Reader (PerkinElmer) with Ex/Em wavelengths at 485 nm/605 nm. PCA and confidence ellipses were obtained with RStudio (Version 1.2.5019), an integrated development environment for R (version 3.6.1). CDA was performed with OriginPro 2018. Classification performance was evaluated by *k*-fold ($k = 8$) cross validation using Python 3, with linear discriminant analysis as the supervised classification model.

Experimental procedures. *Fluorescence measurements.* In general, the fluorescence assay was carried out by mixing 10 μl of the fluorescent guest (6.25 μM **DSMI** or **PSMI** in water), 10 μl of the cavitand (in water) or water, 70 μl of the incubation buffer and 10 μl of 1 μM DNA in a 96-well plate, resulting in a final total volume of around 100 μl in 10 mM K_2HPO_4/KH_2PO_4 (or Na_2HPO_4/NaH_2PO_4) and 1 mM EDTA at pH 7.4. The mixture was incubated with mild shaking for 15 min at room temperature, before the fluorescence signal (F) was recorded on a Perkin Elmer Wallac 1420 Victor 2 Microplate Reader (PerkinElmer) with Ex/Em wavelengths at 485/605 nm.

Array constituents. Type 1 array: hosts **1**–**5** or no host, **DSMI** dye. [**DSMI**] = 0.625 μM, [**1**, **4**, or **5**] = 0.25 μM or [**2** or **3**] = 0.50 μM. Type 2 array: hosts **1**-**5** or no host, **PSMI** dye. [**PSMI**] = 0.625 μM, [**1**, **3**, or **5**] = 0.25 μM, [**2**] = 1.0 μM, or [**4**] = 0.50 μM. 10-component array: combination of Type 1 and Type 2 arrays, not including 'no host'. 12-component array: combination of Type 1 and Type 2 arrays.

Circular dichroism. CD spectra were recorded on a Jasco J-815 CD spectrophotometer over a wavelength range of 200–350 nm at room temperature, with a band width of 1 nm and a data pitch of 1 nm. The instrument scanning speed was set at 100 nm min^{-1}, with a response time of 1 s. To obtain the spectra, 200 μl of 10 μM oligonucleotide solution prepared in the K^+ buffer or Na^+ buffer was pipetted into a quartz cell with a path length of 0.1 cm. The CD spectra are presented with a baseline correction in which the background signal from the buffer was subtracted.

Gel electrophoresis. The quality of the DNA solution was inspected by native gel electrophoresis using a precast gradient (4–20%) PAGE gel. The gel was loaded with 10 μl of a 1 μM DNA solution which had been denatured at 95 °C for 5 min, cooled on ice for 10 min and then held at room temperature for 30 min. The gel was run at 120 V for 90 min at room temperature in 1 × TBE buffer and stained with SYBR Gold (1:10000 dilution) before imaging using a UV transilluminator (SPECTROLINE).

Binding affinity measurements: fluorescence titrations. For hosts **1**–**4**, the fluorescence titration curves were obtained by adding 0–45 μM host **1**–**4** into the solution that contained 0.625 μM **DSMI** or **PSMI** in the K^+ buffer. For host **5**, the titration was carried out in the same manner, by using 0–10 μM host **5** and 10 μM **DSMI** or **PSMI**, because the dye fluorescence was only slightly quenched by the host. Fluorescence was recorded after 15 min of mixing in the plate reader using the instrument setting described above. The binding affinity calculations were performed using the fitting program provided at http://supramolecular.org (ref. [39]). The UV 1:1 filter within the Bindfit program was used along with the Nelder–Mead fitting method[39], with the 'subtract initial value' option selected.

Binding affinity measurements: isothermal titration calorimetry experiments. All isothermal titration calorimetry experiments were performed using a MicroCal iTC200 (GE Healthcare) with a stirring rate of 800 rpm. The baseline was stabilized prior to the experiments and a pre-injection delay was set to 60 s. A stock solution of **DSMI** or **PSMI** at 3 mM in K^+ buffer was added in 2 μl aliquots to the c-myc 2345 solutions of 10 and 40 μM (also in K^+ buffer), respectively. **DSMI** binds about two times more weakly than **PSMI** and thus requires a higher dye/DNA ratio to reach a plateau. All experiments were conducted at 25 °C. The heat of dilution, measured by the injection of titrant into the buffer solution, was subtracted for each titration to obtain the net reaction heat value. Curve fitting was performed with the MicroCal program using the One Set of Sites model.

Discussion of methods: additional points. *Analysis of fluorescence responses.* The fluorescence response titrations shown in Fig. 2a–c are normalized (y axis = F/F_0) to the response of cavitand–dye in the absence of DNA, that is F_0 is defined as the fluorescence recorded for that concentration of host and guest when [DNA] = 0 (purple lines in Extended Data Fig. 2a,c,e). As hosts **1**–**4** cause an enhancement in emission when binding DSMI/PSMI, the raw fluorescence increases variably, depending on host, in each case. Host **5** causes a slight quenching of the dyes upon binding. The unnormalized plots (y axis = fluorescence counts) are shown in Extended Data Fig. 2a,c,e (for **DSMI** and hosts **1**, 2 and **5**) and Supplementary Figs. 18 and 19 (all dye/host combinations). The normalized emission plots allow simple visualization of the effect of the target DNA on the emission profile by removing the effect of the host–dye emission on the signal. The effect of the various DNAs and the mechanism of their sensing is the important point of our study, as the effect of hosts on the dyes is well known[29,31,34,38].

Methods used to calculate binding affinities. The dye•host affinities (Table 1, Supplementary Fig. 14) were measured by fluorescence emission titrations and calculated using the BindFit fitting program available at www.supramolecular.org (ref. [39]). The affinity between the DNA G4 c-myc 2345 and the two dyes was measured by isothermal titration calorimetry (see Supplementary Figs. 15 and 16), as the emission changes were too small for accurate analysis by fluorescence titrations. Determining accurate affinity measurements and the specific location of binding were complicated by the low, multivalent affinity of both dyes for the c-myc 2345 G4, but simple fitting using the OneSites model gave, with approximate binding affinities, of the order of $K_d = 100$–250 μM for both **DSMI** and **PSMI**. The smaller **DSMI** showed a greater multivalency than the larger **PSMI**, albeit with a lower overall affinity. The competitive binding of the dyes to both DNA and hosts is also shown by adding increasing [DNA] to host•dye complexes (see Supplementary Figs. 20 and 21). In this case, the fluorescence increases due to greater [DNA•dye]. The signal changes vary depending on the nature of host, dye and DNA as before.

Data availability

The fluorescence datasets and multivariate analysis data generated in this study are available as Source Data, linked to the corresponding data figures in the online version of this manuscript. The raw data corresponding to the supplementary figures are available as Supplementary Data. Source data are provided with this paper.

Acknowledgements

We thank the National Science Foundation (CHE-1707347 to W.Z and R.J.H.) and MIUR (PRIN 20179BJNA2 to E.D.) for funding.

Author contributions

R.J.H. and W.Z. conceived and designed the experiments and wrote the paper. J.C. performed the arrayed sensing experiments and statistical analysis with help from L.W. and J.L. Chemical synthesis and optical analysis of hosts and dyes were performed by B.L.H., A.D.G, A.F., R.P. and E.D. All authors contributed to manuscript creation and proofreading.

Competing interests

The authors declare no competing interests.

Additional information

Extended data is available for this paper at https://doi.org/10.1038/s41557-021-00647-9.

Supplementary information The online version contains supplementary material available at https://doi.org/10.1038/s41557-021-00647-9.

Correspondence and requests for materials should be addressed to R.J.H.

Peer review information Nature Chemistry thanks the, anonymous, reviewer(s) for their contribution to the peer review of this work.

Reprints and permissions information is available at www.nature.com/reprints.

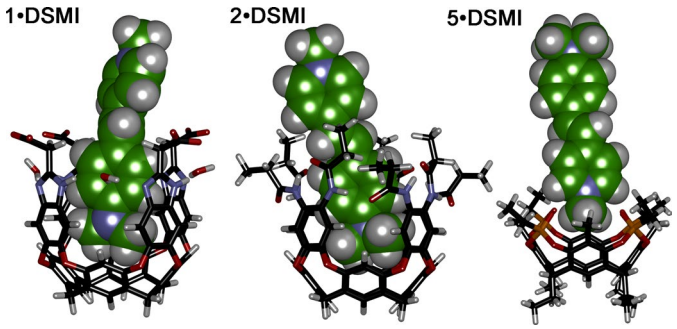

Extended Data Fig. 1 | Host•dye structures. Molecular-minimized structures of three host–guest complexes between guest **DSMI** and hosts **1**, **2** and **5** (SPARTAN, Hartree-Fock). Lower rim substituents removed for clarity.

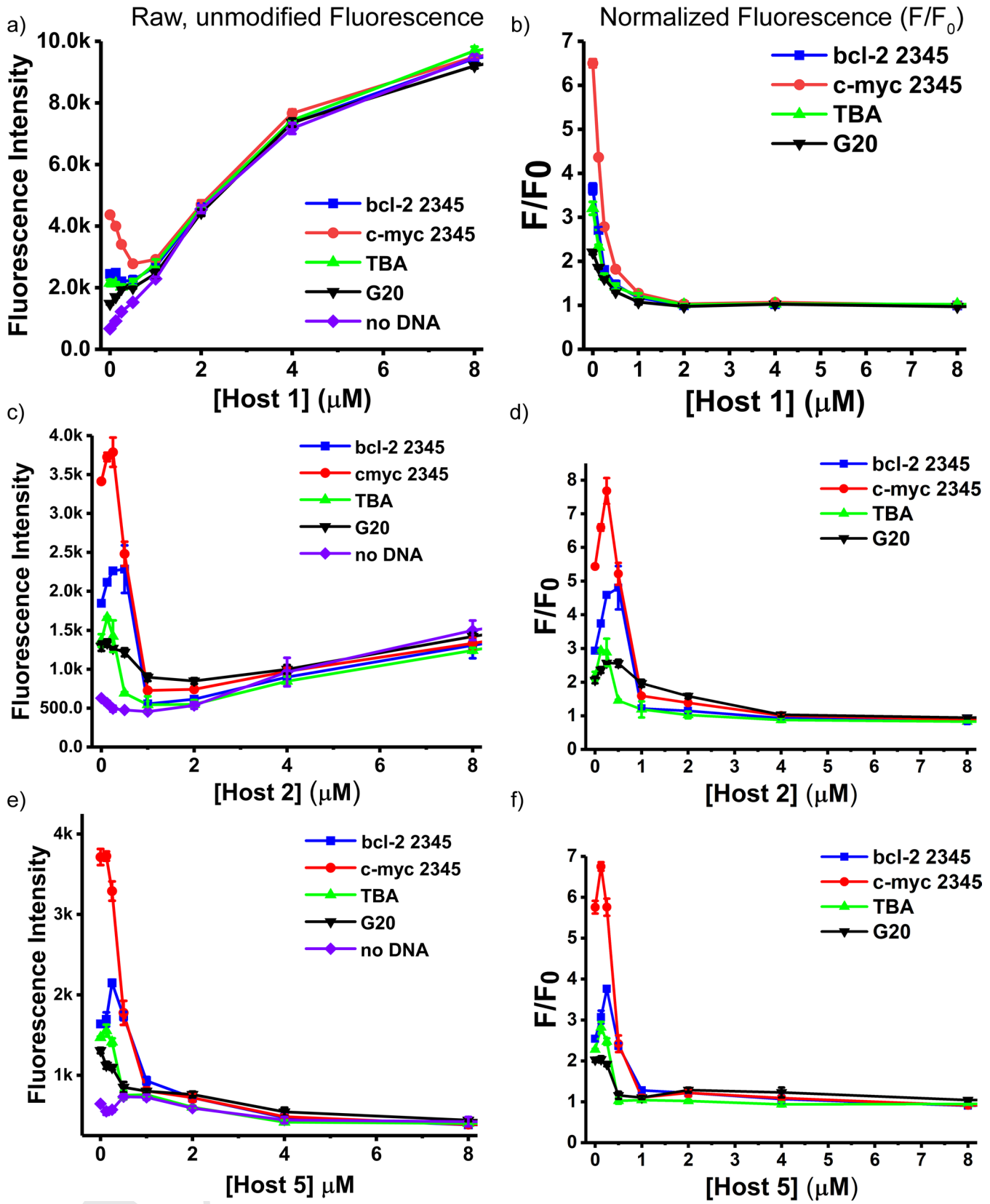

Extended Data Fig. 2 | Effect of DNA strands on the emission profile of various host–dye complexes. Comparison between the raw fluorescence response curves (left) and normalized fluorescence response curves (right) corresponding to the emission of **DSMI** dye in the presence of different DNA strands upon titration of hosts a,b) **1**; c,d) **2**; e,f) **5**, illustrating the effect of the DNA structure on the emission of the various host–guest complexes. [**DSMI**] = 0.625 μM, [DNA] = 0.1 μM, [**host**] = 0-2 μM, 10 mM KH_2PO_4/K_2HPO_4 buffer, 1 mM EDTA, pH 7.4, Ex/Em = 485 nm/605 nm. The normalization process defines F_0 as the emission at [DNA] = 0. Plots a, c, e are extended versions of those shown in Fig. 2. For the full suite of titration plots with all hosts **1-5** and both dyes, see Supplementary Figs. 18 and 19. Error bars represent the standard deviation of 3 repeated measurements.

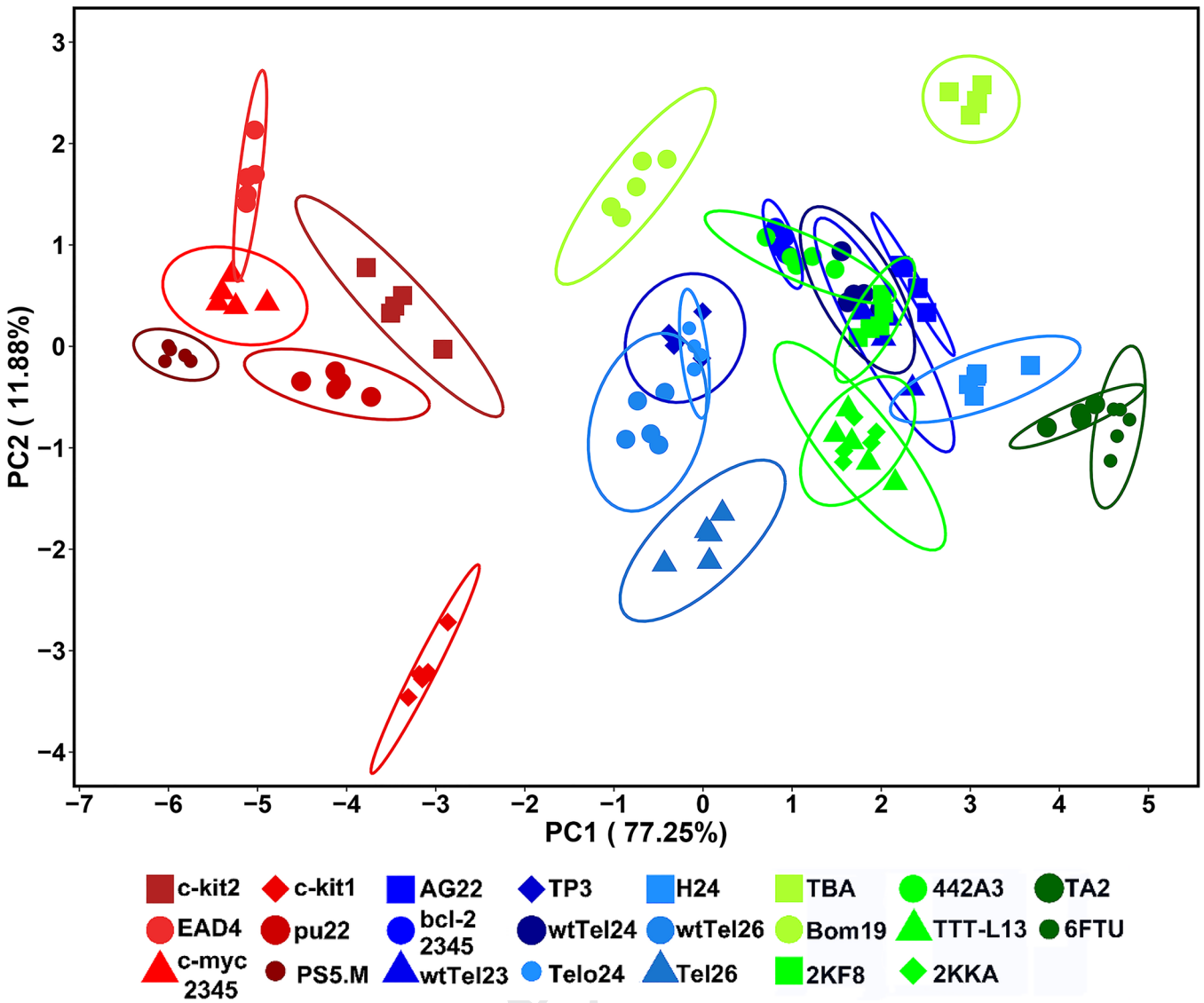

Extended Data Fig. 3 | Discrimination of a suite of 23 G-quadruplex structures. 2D PCA scores plot of the first two principal components (PC) generated from the fluorescence responses of 23 G4 strands to the sensing array. The data is identical to that shown in Fig. 4a, but rather than using the average of 5 repeats for each DNA in PCA, herein each repeat is treated as one individual sample. The first two principal components in total summarize more than 88% of the variation contained in the data, and their scores plot provides a visualization of how the 23 DNA strands are grouped by our array. Ellipses indicate 95% confidence.

QUERY FORM

Nature Chemistry	
Manuscript ID	**[Art. Id: 647]**
Author	**Junyi Chen**

AUTHOR:

The following queries have arisen during the editing of your manuscript. Please answer by making the requisite corrections directly in the e.proofing tool rather than marking them up on the PDF. This will ensure that your corrections are incorporated accurately and that your paper is published as quickly as possible.

Query No.	*Nature of Query*
Q1:	In the sentence beginning 'Multivariate analysis of different...' and elsewhere in the abstract, please confirm that 'G-quadruplex' is OK instead of 'G4'.
Q2:	In the sentence beginning 'As such, there is a need...' please confirm that 'structures' is OK instead of 'structure'.
Q3:	Please check your article carefully, coordinate with any co-authors and enter all final edits clearly in the eproof, remembering to save frequently. Once corrections are submitted, we cannot routinely make further changes to the article.
Q4:	Note that the eproof should be amended in only one browser window at any one time; otherwise changes will be overwritten.
Q5:	Author surnames have been highlighted. Please check these carefully and adjust if the first name or surname is marked up incorrectly. Note that changes here will affect indexing of your article in public repositories such as PubMed. Also, carefully check the spelling and numbering of all author names and affiliations, and the corresponding email address(es).
Q6:	You cannot alter accepted Supplementary Information files except for critical changes to scientific content. If you do resupply any files, please also provide a brief (but complete) list of changes. If these are not considered scientific changes, any altered Supplementary files will not be used, only the originally accepted version will be published.
Q7:	In the e.proof tool, the numbers for those compounds that will be deposited in PubChem do not appear bold, and the link is not visible. You do not need to amend this, they will appear correctly once published online.
Q8:	If applicable, please ensure that any accession codes and datasets whose DOIs or other identifiers are mentioned in the paper are scheduled for public release as soon as possible, we recommend within a few days of submitting your proof, and update the database record with publication details from this article once available.
Q9:	In the sentence beginning 'G4s are generally classified into three different...' please confirm that you are happy with the addition of 'G4' as the definition of 'G-quadruplex'.
Q10:	In the sentence beginning 'As n double-stranded DMA...' please confirm that 'double-stranded DNA' is correct instead of 'dsDNA'.
Q11:	Please confirm that you are happy with the changes to the sentence beginning 'Although computational prediction and...'.

QUERY FORM

Nature Chemistry	
Manuscript ID	**[Art. Id: 647]**
Author	**Junyi Chen**

AUTHOR:

The following queries have arisen during the editing of your manuscript. Please answer by making the requisite corrections directly in the e.proofing tool rather than marking them up on the PDF. This will ensure that your corrections are incorporated accurately and that your paper is published as quickly as possible.

Query No.	*Nature of Query*
Q12:	Please confirm that you are happy with the changes to the caption for Fig. 1.
Q13:	Please note house style is to use (ref. x) in circumstances where a superscript alone may cause ambiguity, for example, on numbers, units and uncommon abbreviations. Please check that you are happy with this throughout the manuscript.
Q14:	House style is that DNAs are written in roman font and genes are in italic font. Please check throughout the manuscript and figures that DNAs and genes are represented correctly and amend as necessary.
Q15:	In the sentence beginning 'Both PSMI and DSMI showed...' please confirm that 'threefold to sixfold' is OK instead of '3–6 fold'
Q16:	Please confirm that you are happy with the changes to the caption for Fig. 2.
Q17:	Please confirm that you are happy with the change to the sentence beginning 'To rationalize...'.
Q18:	Please confirm that you are happy with the changes to the sentence beginning 'The dyes also bind...'.
Q19:	Please confirm that you are happy with the changes to Table 1, including the footnotes.
Q20:	Please confirm that you are happy with the changes to the caption for Fig. 3.
Q21:	In the sentence beginning 'The discrimination is remarkable...' please confirm that 'nt' rather than 'nts" is correct. Please also check other examples throughout the manuscript.
Q22:	Please confirm that you are happy with the change to the sentence beginning 'However, there is significant...'.
Q23:	lease confirm that you are happy with the change to the sentence beginning 'The antiparallel and hybrid G4s...'.
Q24:	Please confirm that you are happy with the changes to the caption for Fig. 4.
Q25:	In the sentence beginning 'To validate this, the responses...' please confirm that 'discriminant' rather than 'discrimination' is correct.
Q26:	Please confirm that you are happy with the changes to the caption for Fig. 5. The value of 'Ex/Em = 485 nm/600 nm' is not the same as the other values of Ex/Em quoted in the text-please check.
Q27:	In the sentence beginning 'The c-myc 2345 G4...' please confirm that 'single-stranded DNA' is OK instead of 'ssDNA'.
Q28:	Please confirm that you are happy with the changes to the sentence beginning 'Our array can even detect changes in G4...'.

QUERY FORM

Nature Chemistry	
Manuscript ID	**[Art. Id: 647]**
Author	**Junyi Chen**

AUTHOR:

The following queries have arisen during the editing of your manuscript. Please answer by making the requisite corrections directly in the e.proofing tool rather than marking them up on the PDF. This will ensure that your corrections are incorporated accurately and that your paper is published as quickly as possible.

Query No.	*Nature of Query*
Q29:	Please confirm that you are happy with the change to the sentence beginning 'This method could potentially...'.
Q30:	Please confirm that you are happy with the change to the sentence beginning 'This could pave the way...'.
Q31:	In the sentence beginning 'NMR spectra were recorded...'. please give the reference compound for the NMR studies.
Q32:	In the sentence beginning 'CDA was performed...' please confirm that 'CDA' is OK instead of 'canonical discriminant analysis'.
Q33:	Please confirm that you are happy with the changes to the 'Circular dichroism' section and also the 'Gel electrophoresis' section.
Q34:	In the sentence beginning 'The UV 1:1: filter...' is 'program' OK instead of 'function'?
Q35:	Please confirm that you are happy with the section heading 'Binding affinity measurements: isothermal titration calorimetry ex[eriments'.
Q36:	Please confirm that you are happy with the section heading 'Discussion of methods: additional points'.
Q37:	In the sentence beginning 'The fluorescence response titrations...' please confirm that Fig. 2a–c should be referred to here.
Q38:	In the sentence beginning 'Determining accurate affinity...' please check that 'OneSites model' is correct